ACS APPLIED MATERIALS & INTERFACES

www.acsami.org

Research Article

Bio-PEDOT: Modulating Carboxyl Moieties in Poly(3,4-ethylenedioxythiophene) for Enzyme-Coupled Bioelectronic Interfaces

Kiattisak Promsuwan, Lingyin Meng, Phachara Suklim, Warakorn Limbut, Panote Thavarungkul, Proespichaya Kanatharana, and Wing Cheung Mak*

Cite This: *ACS Appl. Mater. Interfaces* 2020, 12, 39841−39849

Read Online

ACCESS | Metrics & More | Article Recommendations | Supporting Information

ABSTRACT: Modulation of chemical functional groups on conducting polymers (CPs) provides an effective way to tailor the physicochemical properties and electrochemical performance of CPs, as well as serves as a functional interface for stable integration of CPs with biomolecules for organic bioelectronics (OBEs). Herein, we introduced a facile approach to modulate the carboxylate functional groups on the PEDOT interface through a systematic evaluation on the effect of a series of carboxylate-containing molecules as counterion dopant integrated into the PEDOT backbone, including acetate as monocarboxylate (mono-COO^-), malate as dicarboxylate (di-COO^-), citrate as tricarboxylate (tri-COO^-), and poly(acrylamide-*co*-acrylate) as polycarboxylate (poly-COO^-) bearing different amounts of molecular carboxylate moieties to create tunable PEDOT:COO^- interfaces with improved polymerization efficiency. We demonstrated the modulation of PEDOT:COO^- interfaces with various granulated morphologies from 0.33 to 0.11 μm, tunable surface carboxylate densities from 0.56 to 3.6 μM cm^{-2}, and with improved electrochemical kinetics and cycling stability. We further demonstrated the effective and stable coupling of an enzyme model lactate dehydrogenase (LDH) with the optimized PEDOT:poly-COO^- interface via simple covalent chemistry to develop biofunctionalized PEDOT (Bio-PEDOT) as a lactate biosensor. The biosensing mechanism is driven by a sequential bioelectrochemical signal transduction between the bio-organic LDH and organic PEDOT toward the concept of all-polymer-based OBEs with a high sensitivity of 8.38 μA mM^{-1} cm^{-2} and good reproducibility. Moreover, we utilized the LDH-PEDOT biosensor for the detection of lactate in spiked serum samples with a high recovery value of 91−96% and relatively small RSD in the range of 2.1−3.1%. Our findings provide a new insight into the design and optimization of functional CPs, leading to the development of new OBEs for sensing, biosensing, bioengineering, and biofuel cell applications.

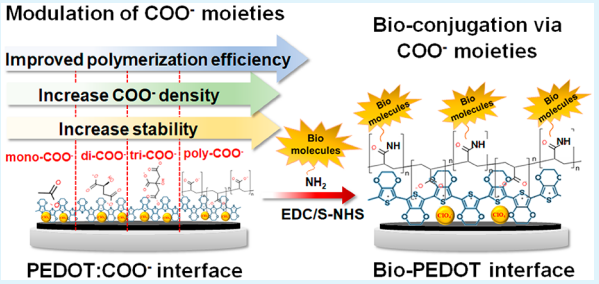

KEYWORDS: *PEDOT, carboxylate functional group, bioelectronic interface, lactate dehydrogenase, lactate biosensor*

1. INTRODUCTION

Organic bioelectronics (OBEs) are emerging electrochemical devices dedicated to specific biological applications including conducting polymers (CPs) coupled with biological molecules with a similar organic nature to biointerfaces bridging the organic electronics and biological systems.[1,2] The unique properties of CPs, such as electronic and ionic conductivities, mechanical flexibility, ease of processing, and sharing similarity in chemical nature with biomolecules (i.e., cell, antibody/antigen, enzyme, etc.), leading to a new concept of all-polymer-based organic/bio-organic devices,[3] overcome the limitations of conventional inorganic material interfaces such as mechanical rigidity, biofouling, and low biocompatibility.[4,5] Among all of the CPs, poly(3,4-ethylenedioxythiophene) (PEDOT) has been considered for use as a biointerfacing material to mediate with biological molecules for cell adhesion,[6] neural stimulation, and recording,[7,8] and sensing and biosensing applications.[9,10] However, the employment of pristine PEDOT as a signal transduction interface between biomolecules has several limitations, such as limited surface area, hysteretic effect, and lack of functional groups.[11] Therefore, tailoring and modulating the functionality of pristine PEDOT to achieve an effective PEDOT biointerface with tunable "affinity" between the PEDOT interface and biomolecules are needed.

Nowadays, several physiochemical strategies have been developed to modulate the PEDOT interface for OBE

Received: June 5, 2020
Accepted: August 6, 2020
Published: August 6, 2020

Downloaded via UTRECHT UNIV on October 8, 2020 at 05:55:24 (UTC).
See https://pubs.acs.org/sharingguidelines for options on how to legitimately share published articles.

© 2020 American Chemical Society

https://dx.doi.org/10.1021/acsami.0c10270
ACS Appl. Mater. Interfaces 2020, 12, 39841−39849

applications. Physical approaches based on the development of PEDOT with specific micro/nanostructure, such as nanodots, nanofibres, microsphere, and porous architecture, endow the PEDOT interface with increased active surface area, resulting in improved cell attachment[12] and biocompatibility for tissue engineering,[13] electrochemical transduction interfaces for biosensors with enhanced sensitivity,[10,14] and high loading capability for electrochemically controlled drug delivery.[15,16] Meanwhile, chemical approaches based on hydrogel-blended PEDOT composites have been widely studied in OBEs. Various PEDOT:hydrogel composites including gelatin,[17] collagen,[18,19] chitosan,[20] and alginate[21] had been reported to modulate the interfacial properties of the PEDOT by incorporating amino acids or polysaccharide moieties via the blended hydrogel to promote cell attachment, growth, and viability in cell biology and bioelectronic applications. Besides blended PEDOT composites, the interfacial properties of PEDOT could be modulated by doping functional dopants/biomolecules into the PEDOT polymer network during the polymerization process. For example, PEDOT interfaces doped with laminin peptides, hyaluronic acid, heparin, and fibrinogen were used to support cell attachment and simultaneously perform electrochemical stimulation to promote neurite growth.[8,12,22] PEDOT doped with laccase was used as a biocathode for fuel cell applications.[23] PEDOT-doped κ-carrageenan and dextran sulfate with enhanced biocompatibility and lower cytotoxicity to support cell culture on the PEDOT interface.[24,25]

A facile and systematic strategy to modulate the PEDOT interface could be achieved via the insertion of chemical functional groups such as carboxylate,[26] amine,[27] and hydroxymethyl.[28] Among them, the insertion and modulation of carboxylate functional groups onto the PEDOT interface provide the most valuable advantage for the development of OBEs that enable effective and stable coupling of PEDOT with a large variety of biofunctional molecules such as the above-mentioned collagen, gelatin, and peptides, as well as biorecognition molecules including nucleic acids, antibodies, and enzymes via well-established covalent chemistry using a range of various coupling agents such as ethyl-(dimethylaminopropyl)carbodiimide (EDC)/*N*-hydroxysulfosuccinimide (sulfo-NHS).[14] Generally, a carboxylate-functionalized PEDOT interface can be prepared by copolymerization of 3,4-ethylenedioxythiophene (EDOT) monomer with its carboxyl derivative EDOT-COOH monomer with a confined ratio.[14,29] However, the slow polymerization efficiency of the EDOT derivative resulted in a relatively low-density carboxyl-functionalized PEDOT interface.[29] Alternatively, another approach involves using carboxylate-containing functional dopants during the EDOT polymerization process, in which the negatively charged carboxylate dopants are inserted into the positively charged backbone of the PEDOT matrix. A variety of carboxylate-containing molecules have been employed as dopants to fabricate carboxylate-functionalized PEDOT interfaces, such as tannic acid,[30] citric acid,[26] hyaluronic acid,[31] sialic acid,[32] bromoisobutyric acid,[33] etc. However, the effects of the carboxylate-containing molecules on the resulting PEDOT interface regarding the carboxylate density, polymerization efficiency, electrochemical properties, and bioconjugation stability, which are critical for optimizing OBE applications, is not well researched to date.

Herein, we introduced a facile approach to modulate the carboxylate functional groups onto the PEDOT interface through a systematic evaluation on the effect of a series of carboxylate containing molecules as counterion dopant integrated into the PEDOT backbone, including acetate (mono-COO^-), malate (di-COO^-), citrate (tri-COO^-), and poly(acrylamide-*co*-acrylate) (poly-COO^-) with different molecular masses and amounts of molecular carboxylate moieties to create tunable PEDOT:COO^- interfaces. The surface morphology, surface carboxylate density, electrochemical properties, and stability of different PEDOT:COO^- interfaces were characterized. We further demonstrate the effective and stable coupling of LDH with the PEDOT:poly-COO^- to fabricate LDH-PEDOT electrochemical lactate biosensor as a model OBE with good analytical performance and demonstrate its application for the detection of lactate in serum sample.

2. EXPERIMENTAL SECTION

2.1. Materials. 3,4-Ethylenedioxythiophene (EDOT), sodium acetate, malic acid disodium salt, sodium citrate dihydrate, poly(acrylamide-*co*-acrylic acid) partial sodium salt (M_w: ∼150 000), lithium perchlorate ($LiClO_4$), *n*-(3-dimethylaminopropyl)-*n*′-ethylcarbodiimide hydrochloride (EDC), toluidine blue O (TBO), *N*-hydroxysulfosuccinimide (sulfo-NHS), sodium L-lactate, L-ascorbic acid (AA), uric acid (UA), dopamine hydrochloride (DA), and glucose were obtained from Sigma-Aldrich (MO). L-Lactate dehydrogenase from rabbit muscle (LDH) and β-nicotinamide adenine dinucleotide reduced disodium salt hydrate (NADH) were purchased from VWR International (Karlskoga, Sweden). Human serum (Type AB) was purchased from PAA Laboratories GmbH (Austria). Potassium hydroxide (KOH), acetic acid (CH_3CO_2H), disodium hydrogen phosphate monohydrate ($Na_2HPO_4{\cdot}H_2O$), and sodium dihydrogen phosphate (NaH_2PO_4) were purchased from Merck (Darmstadt, Germany). Phosphate buffer solutions (PBS, 0.1 M, pH 7.4) were prepared by mixing Na_2HPO_4 and NaH_2PO_4. All chemicals were of analytical grade and used without any further treatment. All solutions were prepared using ultrapure (18.2 MΩ cm) water from a Millipore Milli-Q water purification system (MA).

2.2. Electropolymerization of PEDOT Doped with Carboxylate Groups (PEDOT:COO^-). A glassy carbon electrode (GCE, diameter 3 mm) was carefully polished with 0.30 and 0.05 μm aluminum slurries. After that, the polished GCE was rinsed and sonicated in deionized water and ethanol for 2 min and dried under nitrogen gas. The monomer solution for electropolymerization was prepared by mixing different 10 mM carboxylates as counterion dopants, e.g., acetate (mono-COO^-) (equivalent to 0.82 mg mL^{-1}), malate (di-COO^-) (equivalent to 1.8 mg mL^{-1}), citrate (tri-COO^-) (equivalent to 2.9 mg mL^{-1}), and poly(acrylamide-*co*-acrylate) (poly-COO^-) (equivalent to 5.2 mg mL^{-1}) with 10 mM EDOT monomer and 20 mM $LiClO_4$, followed by sonicating for 30 min. Electropolymerization of PEDOT doped with different carboxylate dopants was carried out in the prepared monomer solution using chronoamperometry at a fixed potential of 1.10 V (vs Ag/AgCl) for 200 s. PEDOT prepared without carboxylate doping was denoted as PEDOT:P, while PEDOT doped with acetate, malate, citrate, and poly(acrylamide-*co*-acrylate) were denoted as PEDOT:mono-COO^-, PEDOT:di-COO^-, PEDOT:tri-COO^-, and PEDOT:poly-COO^-, respectively. The collection of the above carboxylate-doped PEDOT was denoted as PEDOT:COO^-.

2.3. Characterizations of PEDOT:COO^- Interfaces. Indium tin oxide-coated glass (ITO) was used as an alternative working electrode during electropolymerization for the surface characterization experiments. The surface morphologies of PEDOT:P and PEDOT:COO^- interfaces were characterized and recorded by scanning electron microscopy (SEM) using a LEO 155 Gemini (Zeiss, Germany). The carboxylate group on the PEDOT interfaces was characterized using a Fourier transform infrared (FTIR) VERTEX spectrometer (Bruker) equipped with an attenuated total reflection (ATR) measuring cell. To quantify the amount of carboxylate group on the PEDOT:COO^-

https://dx.doi.org/10.1021/acsami.0c10270
ACS Appl. Mater. Interfaces 2020, 12, 39841−39849

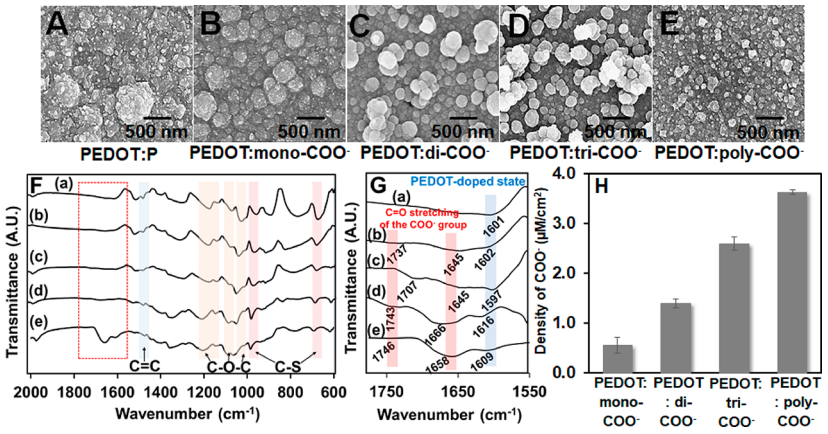

Figure 1. SEM images of different PEDOT:COO$^-$ interfaces: (A) PEDOT:P, (B) PEDOT:mono-COO$^-$, (C) PEDOT:di-COO$^-$, (D) PEDOT:tri-COO$^-$, and (E) PEDOT:poly-COO$^-$; the scale bar is 500 nm. FTIR spectra in the wavenumber range of (F) 2000−600 cm^{-1} and (G) 1750−1550 cm^{-1} for (a) PEDOT:P, (b) PEDOT:mono-COO$^-$, (c) PEDOT:di-COO$^-$, (d) PEDOT:tri-COO$^-$, and (e) PEDOT:poly-COO$^-$. (H) Density of carboxylate groups of different PEDOT:COO$^-$ samples measured by the TBO assay.

electrode surfaces, the TBO staining technique was applied. In brief, various PEDOT:COO$^-$ prepared on ITO substrate with a fixed surface area of 1 cm^2 were incubated in a 2.0 mM TBO solution (0.10 mM KOH) for 2 h. Under alkaline conditions, the negatively charged PEDOT:COO$^-$ bind with the positively charged TBO molecules at a ratio of 1:1.[26,34] Then, nonspecific bound TBO were removed by carefully rinsing the PEDOT:COO$^-$ surface with 0.10 mM KOH. Finally, the samples were immersed in 5 mL of 50% acetic acid for 30 min to allow desorption of TBO molecules from the sample surface. A UV−vis spectrophotometer (UV-2450, Shimadzu, Japan) was used for the qualification of TBO by measuring the absorbance at 631 nm with a standard calibration curve.

2.4. Electrochemical Measurements. All electrochemical measurements were performed by CompactStat potentiostat (Ivium, the Netherlands) and PGSTAT30 potentiostat (Autolab, the Netherlands) with a three-electrode system comprising a glassy carbon electrode as the working electrode, a platinum wire as the counter electrode, and a Ag/AgCl electrode as the reference electrode, respectively. Electrochemical characterizations of the PEDOT:COO$^-$ electrodes were performed using cyclic voltammetry (CV) and electrochemical impedance spectroscopy (EIS). EIS measurements were conducted over the frequency range of 100 kHz to 0.1 Hz with an amplitude of 10 mV at 0.20 V, and the corresponding results were fitted with an equivalent electrical circuit via Nova 2.1 software.

2.5. Biofunctionalization of PEDOT:COO$^-$ (Bio-PEDOT) for Lactate Biosensing. Biofunctionalization of PEDOT:COO$^-$ (Bio-PEDOT) for the preparation of lactate biosensor was done by conjugating the LDH with PEDOT:poly-COO$^-$ via EDC/NHS covalent coupling. In brief, the as-prepared PEDOT:poly-COO$^-$ interface was equilibrated by the CV method with 0.10 M PBS (pH 7.4) for 20 cycles. The equilibrated PEDOT:poly-COO$^-$ was treated with 10 μL of a mixture of 50 mM EDC and 50 mM sulfo-NHS for 1 h to activate the carboxyl groups, followed by washing with 0.10 M PBS (pH 7.4). Then, enzyme LDH was immobilized to the activated PEDOT:poly-COO$^-$ by dropping 10 μL of LDH (10 mg mL^{-1}, 0.10 M PBS, pH 7.4) onto the activated PEDOT:poly-COO$^-$. The LDH-biofunctionalized PEDOT:poly-COO$^-$ (LDH-PEDOT) electrodes were rinsed with buffer (0.10 M PBS, pH 7.4) to remove access reagents. Finally, the LDH-PEDOT electrodes were equilibrated by the CV method with 0.10 M PBS (pH 7.4) for 10 cycles and were employed for lactate measurements. Electrochemical detection of lactate with LDH-PEDOT biosensors was carried out by chronoamperometry in 0.10 M PBS (pH 7.4) containing 5.0 mM NAD$^+$ under stirring using a magnetic bar.

3. RESULTS AND DISCUSSION

3.1. Modulation of PEDOT:COO$^-$ Using Different Carboxylate Dopants. Carboxylate-containing dopants with different carboxylate densities per molecule, including acetate (mono-COO$^-$), malate (di-COO$^-$), citrate (tri-COO$^-$), and poly(acrylamide-*co*-acrylate) (poly-COO$^-$), were used as counterion dopants to modulate the amount of carboxylate moieties integrated into the PEDOT:COO$^-$ interfaces. The polymerization efficiency of PEDOT using these carboxylate-containing dopants for the appearance of $LiClO_4$ was evaluated with potentiostatic polymerization at a fixed potential of 1.1 V, which was chosen as an effective potential for the initiation of EDOT monomer oxidation and polymerization without causing overoxidation.[35−37] As shown in Figure S1, all of the PEDOT samples appeared as a compacted film with a typical dark blue color of PEDOT.[38] The total charge (Q) of the resulting control PEDOT:P and different PEDOT:COO$^-$ was calculated from the potentiostatic polymerization curves with values of 16.70 (PEDOT:P), 17.02 (PEDOT:mono-COO$^-$), 17.00 (PEDOT:di-COO$^-$), 19.70 (PEDOT:tri-COO$^-$), and 20.72 mC (PEDOT:poly-COO$^-$) (Table S1). The thicknesses (d) of these PEDOT films were then calculated according to eq 1[39]

$$d = QM_w/zFA\rho \quad (1)$$

where Q is the charge under electrodeposition, M_w is the molecular weight of EDOT, z = 1 (number of electrons/EDOT unit),[40] A is the area of the electrode, ρ is the specific density of EDOT, and F is Faraday's constant. The film thicknesses for PEDOT:P, PEDOT:mono-COO$^-$, PEDOT:di-COO$^-$, PEDOT:tri-COO$^-$, and PEDOT:poly-COO$^-$ were 2.62, 2.67, 2.67, 3.09, and 3.25 μm, respectively (Table S1). These results show that the total charge and thickness of the PEDOT:COO$^-$ films increase with the increase of carboxylate groups in the dopants, indicating a higher PEDOT polymerization efficiency facilitated by dopants with a higher amount of carboxylate groups.[41,42]

The surface morphologies of the resulting control PEDOT:P and various carboxyl-functionalized PEDOT:COO$^-$ interfaces were investigated by SEM. As shown in Figure 1, all of the PEDOT interfaces are composed of a dense and compact base layer and granules/particles on the surface layer, which is consistent with the instantaneous 2D growth mechanism.[43,44]

https://dx.doi.org/10.1021/acsami.0c10270
ACS Appl. Mater. Interfaces 2020, 12, 39841−39849

The formation of the compact base layer for all of the PEDOT samples is ascribed to the growth and elongation of a soluble oligomer assembled into a dense film during electropolymerization at the electrode surface,[43,44] indicating a good electropolymerization efficiency in the presence of lithium perchlorate as the supporting electrolyte.[4] The granules/particles have different dispersibilities and sizes for various PEDOT surfaces due to the progressive 3D nucleation and growth via the formation of PEDOT branches. For the control PEDOT:P (Figure 1A), its surface morphology exhibited a typical cauliflower-like structure with uneven particle size. In contrast, the surface morphologies of PEDOT:COO$^-$ doped with carboxylate show a distinguished and fairly homogeneously globular structure. On a closer look, the sizes of the globular structures of PEDOT:mono-COO$^-$ (Figure 1B), PEDOT:di-COO$^-$ (Figure 1C), PEDOT:tri-COO$^-$ (Figure 1D), and PEDOT:poly-COO$^-$ (Figure 1E) doped with different types of carboxylate dopants (i.e., dopants with different carboxylate groups per molecule) decreased gradually with an average diameter of 0.33 ± 0.08, 0.21 ± 0.04, 0.18 ± 0.05, and 0.11 ± 0.03 μm, respectively (Figure S2). The improved homogeneity and decreased granular/particle sizes of the PEDOT:COO$^-$ sample are presumably related to the increased formation of PEDOT branches facilitated by the higher density of carboxylate groups during the 3D nucleation and growth progress.[26]

FTIR spectroscopy was used to investigate the chemical characteristics and doping of the carboxylate group in the PEDOT:COO$^-$ film. As shown in Figure 1F(a), the control PEDOT:P shows characteristic bands at 1470 and 1172 cm^{-1} originated from the C=C stretching in the thiophene moiety, and the bands at 1172, 1069, and 1023 cm^{-1} are ascribed to the C−O−C stretching in the ethylenedioxy group,[45,46] while the bands at 953 and 678 cm^{-1} are attributed to the C−S bond stretching.[47] All PEDOT:COO$^-$ samples (Figure 1F(b−e)) show a similar pattern of thiophene characteristic bands with blue-shifting compared to the control PEDOT:P, and the blue-shifting likely resulted from the effect of the carboxylate dopants.[26] Moreover, when considering the FTIR spectra of all of the PEDOT:COO$^-$ in the region ranging from 1750 to 1550 cm^{-1} (Figure 1G(b−e)), the bands appearing at around 1740 and 1650 cm^{-1} were assigned to C=O stretching of the −COO$^-$ group that resulted from the carboxylate dopants.[26,48,49] Moreover, the intensity ratio between the peak intensity of C=O (1650 cm^{-1}) and the peak intensity of C=C (1471 cm^{-1}) that reflects the relative amount of carboxylate moieties of different PEDOT:COO$^-$ was evaluated, as shown in Table S2. The peak intensity ratio of C=O/C=C for PEDOT:mono-COO$^-$, PEDOT:di-COO$^-$, PEDOT:tri-COO$^-$, and PEDOT:poly-COO$^-$ shows an increasing trend consistent with the chemical structures of various carboxylate dopants with an increased amount of carboxylate groups per molecule.

The TBO staining technique was used to quantify the amount of carboxylate groups on different PEDOT:COO$^-$ surfaces.[26,34] Figure 1H shows that the calculated surface densities of carboxylate groups of the PEDOT:mono-COO$^-$, PEDOT:di-COO$^-$, PEDOT:tri-COO$^-$, and PEDOT:poly-COO$^-$ were 0.56 ± 0.08, 1.4 ± 0.1, 2.60 ± 0.04, and 3.6 ± 0.3 μM cm^{-2}, respectively. The result from the TBO assay is consistent with the FTIR result on the peak intensity ratio of C=O/C=C, in which the surface densities of carboxylate groups and the C=O/C=C peak intensity ratios of PEDOT:mono-COO$^-$, PEDOT:di-COO$^-$, PEDOT:tri-COO$^-$, and PEDOT:poly-COO$^-$ show similar increasing trends with a good linear correlation R^2 = 0.9907 (Figure S3). These results demonstrated the successful modulation of the carboxylate density of PEDOT:COO$^-$ using dopants with varying amounts of carboxylate groups per molecule.

3.2. Electrochemical Performances of PEDOT:COO$^-$ Modulated by Carboxylate Density. The electrochemical performance of various PEDOT:COO$^-$ interfaces composed of different amounts of carboxylate groups was evaluated using two differently charged redox probes, i.e., positively charged $Ru(NH_3)_6^{2+/3+}$ and negatively charged $Fe(CN)_6^{3-/4-}$, by CV at a scan rate of 50 mV s^{-1}. Figure S4 shows the CVs of different PEDOT:COO$^-$ interfaces in response to the positively charged $Ru(NH_3)_6^{2+/3+}$ with quasi-reversible redox peaks, and the corresponding peak height currents and peak separations (ΔE_p) that reflect the electrode kinetics were evaluated. Figure 2A summarizes the oxidation peak currents and ΔE_{ps} of the

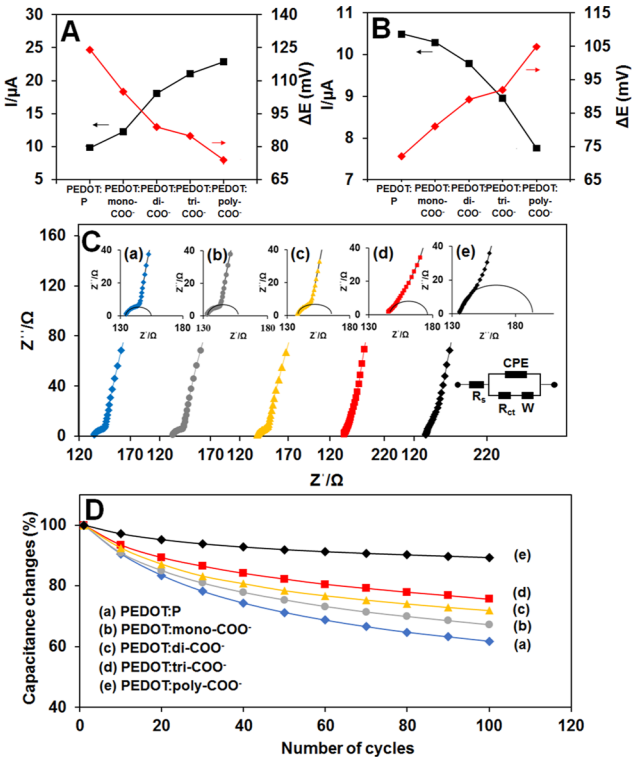

Figure 2. Peak height currents and peak separations (ΔE_p) of the PEDOT:P and the PEDOT:COO$^-$ interfaces recorded in CVs in (A) positively charged $Ru(NH_3)_6^{2+/3+}$ and (B) negatively charged $Fe(CN)_6^{3-/4-}$ in 0.10 M KCl at the scan rate of 50 mV s^{-1}. (C) Nyquist plots fitted with equivalent electrical circuit (inset) and (D) cycling stability of (a) PEDOT:P, (b) PEDOT:mono-COO$^-$, (c) PEDOT:di-COO$^-$, (d) PEDOT:tri-COO$^-$, and (e) PEDOT:poly-COO$^-$.

PEDOT:P, PEDOT:mono-COO$^-$, PEDOT:di-COO$^-$, PEDOT:tri-COO$^-$, and PEDOT:poly-COO$^-$ interfaces modulated by the surface carboxylate density. The oxidation peak currents demonstrated an increasing trend of 9.8, 13.2, 18.1, 21.1, and 22.9 μA as the carboxylate moieties increased in PEDOT:P, PEDOT:mono-COO$^-$, PEDOT:di-COO$^-$, PEDOT:tri-COO$^-$, and PEDOT:poly-COO$^-$, respectively. The oxidation peak current of PEDOT:poly-COO$^-$ is 2.3 times higher than that of the control PEDOT:P (without carboxylate

https://dx.doi.org/10.1021/acsami.0c10270
ACS Appl. Mater. Interfaces 2020, 12, 39841−39849

moieties). Moreover, the ΔE_p value was significantly decreased (1.7 times) from 124 mV for PEDOT:P to 74 mV for PEDOT:poly-COO$^-$. A smaller ΔE_p value indicates a faster electrode kinetics for the PEDOT:COO$^-$ with a higher amount of carboxylate moieties. The increased peak currents and improved electrode kinetics for the PEDOT:COO$^-$ are likely contributed by the negatively charged carboxylate moieties on the PEDOT:COO$^-$ interfaces attracting the positively charged $Ru(NH_3)_6^{2+/3+}$ probe due to electrostatic attraction.[10,26]

In contrast, the CVs of different PEDOT:COO$^-$ interfaces in response to the negatively charged $Fe(CN)_6^{3-/4-}$ are shown in Figure S5, and the corresponding ΔE_p and peak height currents that reflect the electrode kinetics were evaluated. Figure 2B summarizes the oxidation peak current and ΔE_p of the PEDOT:COO$^-$ interfaces. The oxidation peak currents measured from PEDOT:P, PEDOT:mono-COO$^-$, PEDOT:di-COO$^-$, PEDOT:tri-COO$^-$, and PEDOT:poly-COO$^-$ interfaces were 10.5, 10.3, 9.8, 8.9, and 7.7 μA, and the measured ΔE_p values were 72, 81, 89, 92, and 105 mV, respectively. These results further indicate that the effective modulation of carboxylate moiety at the PEDOT:COO$^-$ interfaces bearing negatively charged carboxylate groups hindered the mass transfer of $Fe(CN)_6^{3-/4-}$ due to the electrostatic repulsion effect.[10,26] The electrochemical behaviors of PEDOT:COO$^-$ interfaces in both $Fe(CN)_6^{3-/4-}$ and $Ru(NH_3)_6^{2+/3+}$ probes demonstrated the modulation of PEDOT:COO$^-$ electrode kinetics via the insertion of negatively charged carboxylate dopants with different carboxylate per molecule.

To further investigate the electrochemical properties of various PEDOT:COO$^-$ interfaces, EIS was performed in a 0.10 M KCl solution containing 5.0 mM $Fe(CN)_6^{3-/4-}$, and the corresponding Nyquist plots are shown in Figure 2C. As shown in Figure 2C, all of the Nyquist plots for the PEDOT:COO$^-$ interface composed of a semicircle in the high-frequency region corresponding to the charge transfer process with the semicircle diameter equivalent to the charge transfer resistance (R_{ct}) and a linear part at a low frequency relating to the diffusion process. These Nyquist plots were well fitted with equivalent Randles circuit (inset of Figure 2C), and the parameter values are summarized in Table S3. Compared to the control PEDOT:P electrode (18.38 Ω), the R_{ct} values for the PEDOT:COO$^-$ electrode interfaces showed an apparent increasing trend from 20.43 Ω for PEDOT:mono-COO$^-$ to 65.29 Ω for PEDOT:poly-COO$^-$ interfaces, which can be ascribed to the increased negative charge density on the PEDOT:COO$^-$ interface that hindered the mass transfer of the negatively charged $Fe(CN)_6^{3-/4-}$ probe to the electrode surface by the electrostatic repulsion effect.

To evaluate the stability of the dopants in the PEDOT:COO$^-$ interface, the cycling stabilities of the control PEDOT:P and the PEDOT:COO$^-$ interfaces were investigated by CV scanning in the range between −0.20 and +0.60 V in 0.10 M PBS (pH 7.4) for 100 cycles. The interfacial capacitance values were calculated from CV curves to evaluate the stability of the PEDOT:COO$^-$ interfaces. From the CV curves (Figure S6), we observed that the PEDOT:P showed a decreasing trend with a decrease in the capacitance values as a function of the scanning cycles. This may be caused by the leakage of the low-molecular-weight dopant (i.e., perchlorate) from PEDOT:P. In comparison, all of the PEDOT:COO$^-$ interfaces show improved cycling stability compared to PEDOT:P (Figure 2D). PEDOT:P, PEDOT:mono-COO$^-$, PEDOT:di-COO$^-$, PEDOT:tri-COO$^-$, and PEDOT:poly-COO$^-$ had a cycling stability measured at 100 cycles retaining 61.8, 67.2, 71.8, 75.6, and 89.2% of the initial value, respectively. Moreover, we observed that the cycling stability of the PEDOT:COO$^-$ interfaces increased as the carboxylate groups and the molecular weight (M_w) of the dopants increased (i.e., acetate: M_w = 59, malate: M_w = 133, citrate: M_w = 191, and polycarboxylate: $M_w \sim 150\,000$). This implied that the PEDOT:poly-COO$^-$ doped with polycarboxylate provides the highest stability due to the relatively larger molecular size of polycarboxylate with multiple negatively charged groups that minimized the leakage of dopants from the PEDOT:poly-COO$^-$ matrix.

3.3. Electrochemical Oxidation Behavior of NADH with the PEDOT:poly-COO$^-$. To obtain an optimized carboxylate-functionalized PEDOT for OBE application, a high density of carboxylate functionality and good stability are the two key parameters. Hence, PEDOT:poly-COO$^-$ with the highest carboxylate density and cycling stability was chosen to evaluate its electrochemical transduction behavior toward NADH, which is a prerequisite for the further development of NADH dehydrogenase-based PEDOT biosensors.[10,50] The high density of carboxylate functional groups and the relatively stable PEDOT:poly-COO$^-$ provides an effective interface for covalent coupling of PEDOT:poly-COO$^-$ with biomolecules such as enzyme dehydrogenases, while the PEDOT matrix facilitates the signal transduction for the enzymatic product (i.e., coenzyme-NADH) owing to its high conductivity and reversible redox states.[10,14] The signal transduction behavior for NADH at the PEDOT:poly-COO$^-$ interface was conducted by CV in 0.10 M PBS (pH 7.4) containing 5.0 mM NADH. As shown in Figure 3A, the oxidation peak

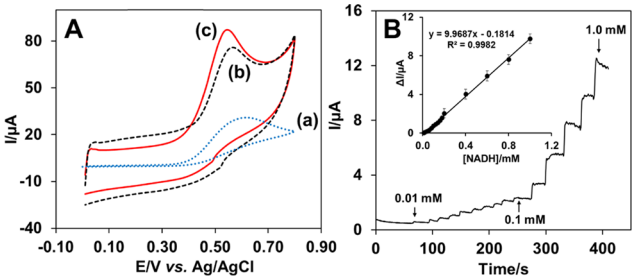

Figure 3. (A) CVs of bare GCE (a), PEDOT:poly-COO$^-$/GCE (b), and PEDOT:poly-COO$^-$-EA/GCE (c) toward 5.0 mM NADH in 0.10 M PBS (pH 7.4) at a scan rate of 50 mV s^{-1}. (B) Chronoamperogram of PEDOT:poly-COO$^-$-EA/GCE toward successive addition of NADH over the range of 0.01−1.0 mM in 0.10 M PBS (pH 7.4) at 0.54 V; the inset shows the corresponding calibration plot.

potential at bare GCE appeared at 0.61 V with a relatively small oxidation peak current of 30.7 μA, while the oxidation peak potential of PEDOT:poly-COO$^-$/GCE negatively shifted to 0.56 V with a significantly larger peak current of 57.9 μA, likely due to the larger electrocatalytic surface area of PEDOT:poly-COO$^-$ with granulated morphology, as indicated by the SEM result. To investigate the net effect on NADH signal transduction by the PEDOT matrix with minimized electrostatic repulsion between the negatively charged carboxylate and NADH at the PEDOT:poly-COO$^-$ interface, ethanolamine was applied to neutralize the surface charge (denoted as PEDOT:poly-COO$^-$-EA/GCE). After the neu-

https://dx.doi.org/10.1021/acsami.0c10270
ACS Appl. Mater. Interfaces 2020, 12, 39841−39849

tralization treatment, the PEDOT:poly-COO$^-$-EA/GCE exhibited the lowest oxidation peak potential at 0.54 V with the highest oxidation peak current of 70.5 μA likely due to the enhanced migration of NADH toward the neutralized PEDOT:poly-COO$^-$-EA/GCE with minimized charge repulsion effect. The electrochemical performance of the PEDOT:poly-COO$^-$-EA/GCE toward NADH determination was evaluated by the successive addition of NADH under stirring at a constant potential of 0.54 V. As shown in Figure 3B, the current response of NADH quickly increased on the successive addition of NADH and reached a steady-state current within 10 s. The corresponding calibration plot between the current responses and NADH concentrations is shown in Figure 3B (inset) with good linearity over the concentration range of 0.01−1.0 mM NADH (R^2 = 0.9982) and a detection sensitivity of 9.97 μA mM^{-1}.

3.4. Bio-PEDOT Organic Polymer-Catalyzed Lactate Biosensor. For OBEs' application, LDH was coupled to the PEDOT:poly-COO$^-$ to fabricate an LDH-PEDOT-based (i.e., Bio-PEDOT) electrochemical lactate biosensor driven by a sequential bioelectrochemical signal transduction mechanism between the bio-organic enzyme and organic PEDOT to demonstrate the concept of all-polymer-based OBEs (Figure 4A). At the LDH-PEDOT interface, LDH catalyzes the conversion of lactate in the presence of NAD$^+$ to pyruvate and NADH, followed by electrochemical oxidation of NADH at the PEDOT interface to generate a current response (Figure 4A). Chronoamperometry was applied for the lactate measurement at LDH-PEDOT in 0.10 M PBS (pH 7.4) containing 5.0 mM NAD$^+$ at 0.54 V. Figure 4B shows that the response current gradually increased with the successive addition of lactate in the concentration ranging from 0.05 to 10 mM. The corresponding calibration plot between the current response and lactate concentration is shown in Figure 4C with good linearity over the concentration range of 0.05−2.0 mM lactate with the regression eq 2 as

$$I_{pa}\ (\mu A) = 0.595 C_{lactate/mM} + 0.022\ (R^2 = 0.9985) \quad (2)$$

and a sensitivity of 8.38 μA mM^{-1} cm^{-2}.

The reproducibility of the LDH-PEDOT fabrication process for the lactate biosensor was evaluated by six repeated measurements with current responses to 0.25, 0.50, and 1.0 mM lactate, as shown in Figure 4D. The relative standard deviation (RSD) values (n = 6) of the individually prepared LDH-PEDOT lactate biosensors were 1.92, 1.62, and 1.10% for 0.25, 0.50, and 1.0 mM lactate, respectively. The measured RSD values were below the AOAC guideline of 5.3%[51] and reveals a good reproducibility. To evaluate the selectivity of the LDH-PEDOT lactate biosensor, the response toward 0.2 mM lactate was tested in the appearance of 0.02 mM AA, 0.1 mM UA, 2.4 nM DA, and 1.0 mM glucose with 5 times dilution of the physiological concentration in normal human serum samples (i.e., 1.0 mM lactate, 0.1 mM AA, 0.5 mM UA, 12 nM DA, and 5.0 mM glucose).[52,53] As shown in Figure 4E, the current signals generated by adding 0.02 mM AA, 0.10 mM UA, 2.4 nM DA, and 1.0 mM glucose were negligible compared to that of 0.2 mM lactate, indicating a good selectivity of the LDH-PEDOT lactate biosensor. To study the possibilities for clinical application, the LDH-PEDOT lactate biosensors were utilized for the determination of lactate in spiked human serum samples. Different concentrations of lactate at 0.50, 1.50, and 5.0 mM were spiked into a 5-fold diluted human serum and measured with the LDH-PEDOT lactate biosensors. As summarized in Table 1, the blank lactate level in the original nonspiked human serum samples was calculated as 1.39 ± 0.12 mM, which is in agreement with the level of lactate in human serum (0.5−1.5 mM). The LDH-PEDOT biosensors for the detection of lactate in spiked serum samples showed good recovery values of 91 ± 2 to 96 ± 2% and small RSD values (n = 3) in the range of 2.1−3.1%. This result suggests that the developed LDH-PEDOT lactate biosensor could be potentially employed for clinical lactate determination.

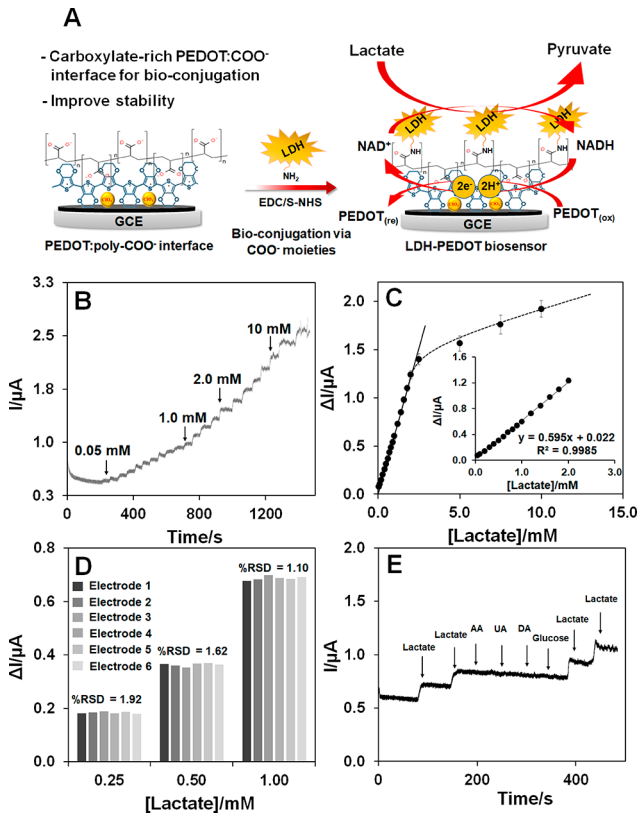

Figure 4. (A) Lactate biosensing mechanism at the LDH-PEDOT interface. (B) Chronoamperogram of LDH/PEDOT:poly-COO$^-$/GCE at 0.54 V for successive injection of lactate in 0.10 M PBS (pH 7.4) containing 5.0 mM NAD$^+$. (C) Calibration plot of the current response against lactate concentration in the range of 0.05−10 mM (n = 3); the inset shows the corresponding linear calibration curve in the range of 0.05−2.0 mM. (D) Reproducibility of six LDH/PEDOT:poly-COO$^-$/GCE responses to 0.25, 0.5, and 1.0 mM lactate. (E) Selectivity of the LDH/PEDOT:poly-COO$^-$/GCE for the detection of lactate in the appearance of AA, UA, DA, and glucose.

4. CONCLUSIONS

We have demonstrated a facile approach to modulate the polymerization efficiency, surface carboxylate density, electrode kinetics, and stability of PEDOT:COO$^-$ interfaces by doping common organic acids including acetate (mono-COO$^-$), malate (di-COO$^-$), citrate (tri-COO$^-$), and poly(acrylamide-*co*-acrylate) (poly-COO$^-$) with different amounts of carboxylate functional groups and molecular weight. We observed that the polymerization efficiency, surface carboxylate density, electrochemical kinetics, and cycling stability of the resulting PEDOT:COO$^-$ interfaces increased as the molecular weight and carboxylate groups of the organic acid dopants

https://dx.doi.org/10.1021/acsami.0c10270
ACS Appl. Mater. Interfaces 2020, 12, 39841−39849

Table 1. Determination of Lactate in Human Serum Samples and Recovery of the Spiking Measured by the Proposed Lactate Biosensor (n = 3)

samples	spiked concentration (mM)	determined concentration (mM)	calculated concentration (mM)	% recovery	% RSD
human serum samples	0	1.39 ± 0.12			
	0.5	1.87 ± 0.02	0.48 ± 0.02	95 ± 3	3.1
	1.5	2.83 ± 0.03	1.44 ± 0.03	96 ± 2	2.1
	5.0	5.95 ± 0.10	4.56 ± 0.10	91 ± 2	2.2

increased, which is likely attributed to the increased doping efficiency and minimized leakage of high-molecular-weight poly(acrylamide-*co*-acrylate) from the PEDOT:poly-COO^- matrix. For OBEs application, the PEDOT:poly-COO^- interface showed a good NADH electrocatalytic activity with a wider linear range and higher sensitivity. Moreover, the carboxylate groups on the PEDOT:poly-COO^- interface served as intermediate anchoring sites for stable covalent coupling of enzyme LDH for the fabrication of LDH-PEDOT biosensors for lactate detection with high sensitivity, good selectivity, and reproducibility. Moreover, we demonstrated the application of the LDH-PEDOT biosensors for lactate detection in a spiked human serum sample with good recovery values. These findings provide new insight into the effects of organic acid dopants for tailoring and modulation of the carboxylate functionality of PEDOT, which are critical for the future development of advanced PEDOT-based OBE devices for biosensing, biomedical, bioengineering, and energy applications.

■ ASSOCIATED CONTENT

Supporting Information

The Supporting Information is available free of charge at https://pubs.acs.org/doi/10.1021/acsami.0c10270.

Images of electrochemical polymerized PEDOT:COO^- films, size distribution of the globular structures of PEDOT:COO^-, correlation plot between TBO and FTIR results, CV of PEDOT:COO^- in $Ru(NH_3)_6^{2+/3+}$ and $Fe(CN)_6^{3-/4-}$, cycling stability of PEDOT:COO^-, total charge and film thickness of PEDOT:COO^-, FTIR peak intensity ratio of PEDOT:COO^-, and fitted parameters obtained by the EIS spectra of PEDOT:-COO^- (PDF)

■ AUTHOR INFORMATION

Corresponding Author

Wing Cheung Mak − *Biosensors and Bioelectronics Centre, Department of Physics, Chemistry and Biology, Linköping University, SE-581 83 Linköping, Sweden;* orcid.org/0000-0003-3274-6029; Phone: +46(0)13 28 6921; Email: wing.cheung.mak@liu.se

Authors

Kiattisak Promsuwan − *Biosensors and Bioelectronics Centre, Department of Physics, Chemistry and Biology, Linköping University, SE-581 83 Linköping, Sweden; Center of Excellence for Trace Analysis and Biosensor and Department of Chemistry, Faculty of Science, Prince of Songkla University, Hat Yai, Songkhla 90112, Thailand*

Lingyin Meng − *Biosensors and Bioelectronics Centre, Department of Physics, Chemistry and Biology, Linköping University, SE-581 83 Linköping, Sweden*

Phachara Suklim − *Biosensors and Bioelectronics Centre, Department of Physics, Chemistry and Biology, Linköping University, SE-581 83 Linköping, Sweden; Center of Excellence for Trace Analysis and Biosensor and Department of Physics, Faculty of Science, Prince of Songkla University, Hat Yai, Songkhla 90112, Thailand*

Warakorn Limbut − *Center of Excellence for Trace Analysis and Biosensor and Department of Applied Science, Faculty of Science, Prince of Songkla University, Hat Yai, Songkhla 90112, Thailand*

Panote Thavarungkul − *Center of Excellence for Trace Analysis and Biosensor and Department of Physics, Faculty of Science, Prince of Songkla University, Hat Yai, Songkhla 90112, Thailand;* orcid.org/0000-0002-6096-6371

Proespichaya Kanatharana − *Center of Excellence for Trace Analysis and Biosensor and Department of Chemistry, Faculty of Science, Prince of Songkla University, Hat Yai, Songkhla 90112, Thailand*

Complete contact information is available at: https://pubs.acs.org/10.1021/acsami.0c10270

Notes

The authors declare no competing financial interest.

■ ACKNOWLEDGMENTS

The authors acknowledge the Swedish Research Council (VR-2015-04434) and Thailand Science Research and Innovation (TSRI) (IRN62W0002) for financial support to conduct the research. They also acknowledge the financial support for K.P. from the Royal Golden Jubilee Ph.D program (RGJ) from the Thailand Research Fund (PHD/0212/2559) and financial support for P.S. from the Development and Promotion of Science and Technology Talents projects (DPST) from the Royal Thai Government.

■ REFERENCES

(1) Richter-Dahlfors, A.; Berggren, M. Organic Bioelectronics. In *Encyclopedia of Nanotechnology*; Bhushan, B., Ed.; Springer Netherlands: Dordrecht, 2012; pp 2014−2022.

(2) Simon, D.; Gabrielsson, E.; Tybrandt, K.; Berggren, M. Organic Bioelectronics: Bridging the Signaling Gap between Biology and Technology. *Chem. Rev.* **2016**, *116*, 13009−13041.

(3) Inal, S.; Rivnay, J.; Suiu, A. O.; Malliaras, G. G.; McCulloch, I. Conjugated Polymers in Bioelectronics. *Acc. Chem. Res* **2018**, *51*, 1368−1376.

(4) Feron, K.; Lim, R.; Sherwood, C.; Keynes, A.; Brichta, A.; Dastoor, P. Organic Bioelectronics: Materials and Biocompatibility. *Int. J. Mol. Sci.* **2018**, *19*, 2382.

(5) Löffler, S.; Libberton, B.; Richter-Dahlfors, A. Organic Bioelectronic Tools for Biomedical Applications. *Electronics* **2015**, *4*, 879−908.

(6) Stewart, E. M.; Fabretto, M.; Mueller, M.; Molino, P. J.; Griesser, H. J.; Short, R. D.; Wallace, G. G. Cell Attachment and Proliferation on High Conductivity PEDOT−Glycol Composites Produced by Vapour Phase Polymerisation. *Biomater. Sci.* **2013**, *1*, 368−378.

(7) Carli, S.; Bianchi, M.; Zucchini, E.; Di Lauro, M.; Prato, M.; Murgia, M.; Fadiga, L.; Biscarini, F. Electrodeposited PEDOT:Nafion

Composite for Neural Recording and Stimulation. *Adv. Healthcare Mater.* **2019**, *8*, No. 1900765.
(8) Asplund, M.; Holst, H.; Inganas, O. Composite Biomolecule/PEDOT Materials for Neural Electrodes. *Biointerphases* **2008**, *3*, 83−93.
(9) Liu, Y.; Turner, A. P. F.; Zhao, M.; Mak, W. C. Processable Enzyme-Hybrid Conductive Polymer Composites for Electrochemical Biosensing. *Biosens. Bioelectron.* **2018**, *100*, 374−381.
(10) Meng, L.; Turner, A. P. F.; Mak, W. C. Positively-Charged Hierarchical PEDOT Interface with Enhanced Electrode Kinetics for NADH-Based Biosensors. *Biosens. Bioelectron.* **2018**, *120*, 115−121.
(11) Xia, L.; Wei, Z.; Wan, M. Conducting Polymer Nanostructures and Their Application in Biosensors. *J. Colloid Interface Sci.* **2010**, *341*, 1−11.
(12) Bhagwat, N.; Murray, R. E.; Shah, S. I.; Kiick, K. L.; Martin, D. C. Biofunctionalization of PEDOT Films with Laminin-Derived Peptides. *Acta Biomater.* **2016**, *41*, 235−246.
(13) Guex, A. G.; Puetzer, J. L.; Armgarth, A.; Littmann, E.; Stavrinidou, E.; Giannelis, E. P.; Malliaras, G. G.; Stevens, M. M. Highly Porous Scaffolds of PEDOT:PSS for Bone Tissue Engineering. *Acta Biomater.* **2017**, *62*, 91−101.
(14) Meng, L.; Turner, A. P. F.; Mak, W. C. Tunable 3D Nanofibrous and Bio-Functionalised PEDOT Network Explored as a Conducting Polymer-Based Biosensor. *Biosens. Bioelectron.* **2020**, *159*, No. 112181.
(15) Yasin, M. N.; Brooke, R. K.; Rudd, S.; Chan, A.; Chen, W.-T.; Waterhouse, G. I. N.; Evans, D.; Rupenthal, I. D.; Svirskis, D. 3-Dimensionally Ordered Macroporous PEDOT Ion-Exchange Resins Prepared byVapor Phase Polymerization for Triggered Drug Delivery: Fabrication and Characterization. *Electrochim. Acta* **2018**, *269*, 560−570.
(16) Boehler, C.; Asplund, M. A Detailed Insight into Drug Delivery from PEDOT Based on Analytical Methods: Effects and Side Effects. *J. Biomed. Mater. Res. A* **2015**, *103*, 1200−1207.
(17) Bongo, M.; Winther-Jensen, O.; Himmelberger, S.; Strakosas, X.; Ramuz, M.; Hama, A.; Stavrinidou, E.; Malliaras, G.; Salleo, A.; Winther-Jensen, B.; Owens, R. PEDOT:Gelatin Composites Mediate Brain Endothelial Cell Adhesion. *J. Mater. Chem. B* **2013**, *1*, 3860−3867.
(18) Xiao, Y.; Li, C. M.; Wang, S.; Shi, J.; Ooi, C. P. Incorporation of Collagen in Poly(3,4-Ethylenedioxythiophene) for a Bifunctional Film with High Bio- and Electrochemical Activity. *J. Biomed. Mater. Res. A* **2010**, *92*, 766−772.
(19) Inal, S.; Hama, A.; Ferro, M.; Pitsalidis, C.; Oziat, J.; Iandolo, D.; Pappa, A.-M.; Hadida, M.; Huerta, M.; Marchat, D.; Mailley, P.; Owens, R. M. Conducting Polymer Scaffolds for Hosting and Monitoring 3D Cell Culture. *Adv. Biosyst.* **2017**, *1*, No. 1700052.
(20) Abedi, A.; Hasanzadeh, M.; Tayebi, L. Conductive Nanofibrous Chitosan/PEDOT:PSS Tissue Engineering Scaffolds. *Mater. Chem. Phys.* **2019**, *237*, No. 121882.
(21) Ferlauto, L.; D'Angelo, A. N.; Vagni, P.; Airaghi Leccardi, M. J. I.; Mor, F. M.; Cuttaz, E. A.; Heuschkel, M. O.; Stoppini, L.; Ghezzi, D. Development and Characterization of PEDOT:PSS/Alginate Soft Microelectrodes for Application in Neuroprosthetics. *Front. Neurosci.* **2018**, *12*, 648.
(22) Green, R. A.; Lovell, N. H.; Poole-Warren, L. A. Impact of Co-Incorporating Laminin Peptide Dopants and Neurotrophic Growth Factors on Conducting Polymer Properties. *Acta Biomater.* **2010**, *6*, 63−71.
(23) Li, Y.; Chen, S.-M.; Wu, T. Y.; Ku, S. H.; Ajmal Ali, M.; AlHemaid, F. Immobilization of Laccase into Poly(3,4-Ethylenedioxythiophene) Assisted Biocathode for Biofuel Cell Applications. *Int. J. Electrochem. Sci.* **2012**, *7*, 11400−11413.
(24) Zamora-Sequeira, R.; Ardao, I.; Starbird, R.; García-González, C. A. Conductive Nanostructured Materials Based on Poly (3,4-Ethylenedioxythiophene) (PEDOT) and Starch/K-Carrageenan for Biomedical Applications. *Carbohydr. Polym.* **2018**, *189*, 304−312.
(25) Harman, D. G.; Gorkin, R.; Stevens, L.; Thompson, B.; Wagner, K.; Weng, B.; Chung, J. H. Y.; in het Panhuis, M.; Wallace, G. G. Poly (3,4-Ethylenedioxythiophene):Dextran Sulfate (PEDOT:DS) − A Highly Processable Conductive Organic Biopolymer. *Acta Biomater.* **2015**, *14*, 33−42.
(26) Meng, L.; Turner, A. P. F.; Mak, W. C. Modulating Electrode Kinetics for Discrimination of Dopamine by a PEDOT:COOH Interface Doped with Negatively Charged Tricarboxylate. *ACS Appl. Mater. Interfaces* **2019**, *11*, 34497−34506.
(27) Sappia, L. D.; Piccinini, E.; von Binderling, C.; Knoll, W.; Marmisollé, W.; Azzaroni, O. PEDOT-Polyamine Composite Films for Bioelectrochemical Platforms - Flexible and Easy to Derivatize. *Mater. Sci. Eng., C* **2020**, *109*, No. 110575.
(28) Daprà, J.; Lauridsen, L. H.; Nielsen, A. T.; Rozlosnik, N. Comparative Study on Aptamers as Recognition Elements for Antibiotics in a Label-Free All-Polymer Biosensor. *Biosens. Bioelectron.* **2013**, *43*, 315−320.
(29) Luo, S.-C.; Mohamed Ali, E.; Tansil, N. C.; Yu, H.-h.; Gao, S.; Kantchev, E. A. B.; Ying, J. Y. Poly (3,4-Ethylenedioxythiophene) (PEDOT) Nanobiointerfaces: Thin, Ultrasmooth, and Functionalized PEDOT Films with in Vitro and in Vivo Biocompatibility. *Langmuir* **2008**, *24*, 8071−8077.
(30) Chen, L.; Lv, S.; Gao, Z.; Chen, C. Voltammetric Immunoassay for the Carcinoembryonic Antigen by Using a Glassy Carbon Electrode Modified with Poly (3,4-Ethylenedioxythiophene) Doped with Tannic Acid and Grafted with Poly (Ethylene glycol). *Microchim. Acta* **2017**, *184*, 4705−4712.
(31) Wang, W.; Cui, M.; Song, Z.; Luo, X. An Antifouling Electrochemical Immunosensor for Carcinoembryonic Antigen Based on Hyaluronic Acid Doped Conducting Polymer PEDOT. *RSC Adv.* **2016**, *6*, 88411−88416.
(32) Hai, W.; Goda, T.; Takeuchi, H.; Yamaoka, S.; Horiguchi, Y.; Matsumoto, A.; Miyahara, Y. Specific Recognition of Human Influenza Virus with PEDOT Bearing Sialic Acid-Terminated Trisaccharides. *ACS Appl. Mater. Interfaces* **2017**, *9*, 14162−14170.
(33) Zhao, H.; Zhu, B.; Luo, S.-C.; Lin, H.-A.; Nakao, A.; Yamashita, Y.; Yu, H.-h. Controlled Protein Absorption and Cell Adhesion on Polymer-Brush-Grafted Poly(3,4-ethylenedioxythiophene) Films. *ACS Appl. Mater. Interfaces* **2013**, *5*, 4536−4543.
(34) Hosseini, S.; Ibrahim, F.; Djordjevic, I.; Koole, L. H. Polymethyl Methacrylate-Co-Methacrylic Acid Coatings with Controllable Concentration of Surface Carboxyl Groups: A Novel Approach in Fabrication of Polymeric Platforms for Potential Bio-Diagnostic Devices. *Appl. Surf. Sci.* **2014**, *300*, 43−50.
(35) Du, X.; Wang, Z. Effects of Polymerization Potential on the Properties of Electrosynthesized PEDOT Films. *Electrochim. Acta* **2003**, *48*, 1713−1717.
(36) Kakhki, S.; Barsan, M. M.; Shams, E.; Brett, C. M. A. Development and Characterization of Poly(3,4-Ethylenedioxythiophene)-Coated Poly(methylene blue)-Modified Carbon Electrodes. *Synth. Met.* **2012**, *161*, 2718−2726.
(37) Pigani, L.; Heras, A.; Colina, Á.; Seeber, R.; López-Palacios, J. Electropolymerisation of 3,4-Ethylenedioxythiophene in Aqueous Solutions. *Electrochem. Commun.* **2004**, *6*, 1192−1198.
(38) Sindhu, S.; Narasimha Rao, K.; Ahuja, S.; Kumar, A.; Gopal, E. S. R. Spectral and Optical Performance of Electrochromic Poly(3,4-Ethylenedioxythiophene) (PEDOT) Deposited on Transparent Conducting Oxide Coated Glass and Polymer Substrates. *Mater. Sci. Eng. B* **2006**, *132*, 39−42.
(39) Qin, Q.; Guo, Y. Preparation and Characterization of Nano-Polyaniline Film on ITO Conductive Glass by Electrochemical Polymerization. *J. Nanomater.* **2012**, *2012*, No. 519674.
(40) Chen, T.-W.; Tsai, T.-H.; Chen, S.-M.; Lin, K.-C. Using PEDOT Film Modified Electrode to Monitor Iodide and Its Enhancement of Arsenite Sensing. *Int. J. Electrochem. Sci.* **2011**, *6*, 2043−2057.
(41) Seki, Y.; Takahashi, M.; Takashiri, M. Effects of Different Electrolytes and Film Thicknesses on Structural and Thermoelectric Properties of Electropolymerized Poly(3,4-Ethylenedioxythiophene) Films. *RSC Adv.* **2019**, *9*, 15957−15965.

https://dx.doi.org/10.1021/acsami.0c10270
ACS Appl. Mater. Interfaces 2020, 12, 39841−39849

(42) Del-Oso, J. A.; Frontana-Uribe, B. A.; Maldonado, J.-L.; Rivera, M.; Tapia-Tapia, M.; Roa-Morales, G. Electrochemical Deposition of Poly[Ethylene-dioxythiophene] (PEDOT) Films on ITO Electrodes for Organic Photovoltaic Cells:Control of Morphology, Thickness, and Electronic Properties. *J. Solid State Chem.* **2018**, *22*, 2025−2037.
(43) Pringle, J. M.; Armel, V.; MacFarlane, D. R. Electrodeposited PEDOT-on-Plastic Cathodes for Dye-Sensitized Solar Cells. *Chem. Commun.* **2010**, *46*, 5367−5369.
(44) Pringle, J. M.; Forsyth, M.; MacFarlane, D. R.; Wagner, K.; Hall, S. B.; Officer, D. L. The Influence of the Monomer and the Ionic Liquid on the Electrochemical Preparation of Polythiophene. *Polymer* **2005**, *46*, 2047−2058.
(45) Nie, T.; Xu, J.-K.; Lu, L.-M.; Zhang, K.-X.; Bai, L.; Wen, Y.-P. Electroactive species-Doped Poly (3,4-Ethylenedioxythiophene) Films: Enhanced Sensitivity for Electrochemical Simultaneous Determination of Vitamins B2, B6 and C. *Biosens. Bioelectron.* **2013**, *50*, 244−250.
(46) Nie, T.; Leng, J.; Bai, L.; Lu, L.; Xu, J.; Zhang, K. Synthesis and Characterization of Benzenesulfonate Derivatives Doped Poly (3,4-Ethylenedioxythiophene) Films and Their Application in Electrocatalysis. *Synth. Met.* **2014**, *189*, 161−172.
(47) Kvarnström, C.; Neugebauer, H.; Blomquist, S.; Ahonen, H. J.; Kankare, J.; Ivaska, A.; Sariciftci, N. S. In Situ FTIR Spectroelectrochemical Characterization of Poly (3,4-Ethylenedioxythiophene) Films. *Synth. Met.* **1999**, *101*, 66.
(48) Povlich, L. K.; Cho, J. C.; Leach, M. K.; Corey, J. M.; Kim, J.; Martin, D. C. Synthesis, Synthesis, Copolymerization and Peptide-Modification of Carboxylic Acid-Functionalized 3,4-Ethylenedioxythiophene (EDOTacid) for Neural Electrode Interfaces. *Biochim. Biophys. Acta* **2013**, *1830*, 4288−4293.
(49) Ostrovsky, S.; Hahnewald, S.; Kiran, R.; Mistrik, P.; Hessler, R.; Tscherter, A.; Senn, P.; Kang, J.; Kim, J.; Roccio, M.; Lellouche, J. P. Conductive Hybrid Carbon Nanotube (CNT)−Polythiophene Coatings for Innovative Auditory Neuron-Multi-Electrode Array Interfacing. *RSC Adv.* **2016**, *6*, 41714−41723.
(50) Omar, F. S.; Duraisamy, N.; Ramesh, K.; Ramesh, S. Conducting Polymer and Its Composite Materials Based Electrochemical Sensor for Nicotinamide Adenine Dinucleotide (NADH). *Biosens. Bioelectron.* **2016**, *79*, 763−775.
(51) AOAC. Appendix F: Guidelines for Standard Method Performance Requirements. Official Methods of Analysis of AOAC International 2016, 20th Edition.
(52) Promsuwan, K.; Kachatong, N.; Limbut, W. Simple Flow Injection System for Non-Enzymatic Glucose Sensing Based on an Electrode Modified with Palladium Nanoparticles-Graphene Nanoplatelets/Mullti-Walled Carbon Nanotubes. *Electrochim. Acta* **2019**, *320*, No. 134621.
(53) Burtis, C. A.; Ashwood, E. R.; Bruns, D. E. *Tietz Textbook of Clinical Chemistry and Molecular Diagnostics*, 4th ed.; Saunders Elsevier: Missouri, 2006.

https://dx.doi.org/10.1021/acsami.0c10270
ACS Appl. Mater. Interfaces 2020, 12, 39841−39849